Online Adaptive Parameter Identification and State-of-Charge Coestimation for Lithium-Polymer Battery Cells

Habiballah Rahimi-Eichi, *Student Member, IEEE*, Federico Baronti, *Member, IEEE*, and Mo-Yuen Chow, *Fellow, IEEE*

***Abstract*—Real-time estimation of the state of charge (SOC) of the battery is a crucial need in the growing fields of plug-in hybrid electric vehicles and smart grid applications. The accuracy of the estimation algorithm directly depends on the accuracy of the model used to describe the characteristics of the battery. Considering a resistance–capacitance (RC)-equivalent circuit to model the battery dynamics, we use a piecewise linear approximation with varying coefficients to describe the inherently nonlinear relationship between the open-circuit voltage $(V_{\rm OC})$ and the SOC of the battery. Several experimental test results on lithium (Li)-polymer batteries show that not only do the $V_{\rm OC}$–SOC relationship coefficients vary with the SOC and charging/discharging rates but also the RC parameters vary with them as well. The moving window least squares parameter-identification technique was validated by both data obtained from a simulated battery model and experimental data. The necessity of updating the parameters is evaluated using observers with updating and nonupdating parameters. Finally, the SOC coestimation method is compared with the existing well-known SOC estimation approaches in terms of performance and accuracy of estimation.**

***Index Terms*—Battery modeling, observer, open-circuit voltage, parameter identification, piecewise linearization, state-of-charge (SOC) estimation.**

I. Introduction

THE battery, as the most prominent energy-storage device, holds promising potential for the realization of the rapidly evolving smart grid concept and electrified transportation systems. Battery technology is growing very quickly to produce cells with higher energy and power densities and to reduce costs. Major developments have been achieved in lithium-ion (Li-ion) battery technology. Among the different flavors of this technology, lithium-polymer cells emerge for their very high energy and power densities, making them very attractive for plug-in hybrid electric vehicles (PHEVs) and in general electric vehicle (EV) use to improve the driving range of an EV. However, the cost efficiency and reliability of the battery in different applications directly depend on the algorithms applied to perform energy and battery management. The urgent prerequisite of these algorithms for making optimal decisions is to have an accurate estimation of the battery state of charge (SOC) and state of health (SOH).

Among the different approaches to estimate the SOC, coulomb counting (Ah counting) [1] is one of the most conventional. However, it suffers from the unknown initial value for the SOC and the accumulated error over time due to the integration process. Although current sensors with high accuracy are available, the error can be caused by different sources, such as data acquisition process, noise, or analog-to-digital resolution, with accumulation effect from the integration process. On the other side, measuring the open-circuit voltage $(V_{\rm OC})$ is another approach that can be used independently [2] or in combination with coulomb counting [3]. However, this method is inappropriate for online applications, as $V_{\rm OC}$ measurement requires the battery to be in the relaxation mode for a long time (in the range of hours). Similarly, electrochemical impedance spectroscopy, which uses the battery's internal impedance to estimate the SOC [4], [5], is only suitable for offline applications. That is why observer-based techniques, such as the Kalman filter [6]–[9], the sliding mode [10]–[12], or H_∞ [13], have been developed and have become popular recently to compensate for the overpotential dynamics of the battery and to calculate the SOC based on the estimated $V_{\rm OC}$. Although these techniques use robust recursive tools to consider nonlinearities and uncertainties in the battery model, they are all designed based on offline identification of the battery model's parameters. Considering fixed parameters for the battery model is an assumption that contradicts the experimental and analytical results of modeling different batteries at different SOCs and various environmental conditions. As shown in [14], some parameters of the battery model change as much as 800% without a change in temperature or discharging current rate when the SOC fluctuates between 0% and 100%.

The method we propose here to estimate the SOC is based on considering a simple resistance–capacitance (RC)-equivalent circuit to model the battery dynamics while using an adaptive online parameter-identification algorithm to identify and update the model's parameters as they change. We deploy a piecewise linearized mapping of the $V_{\rm OC}$–SOC curve along with continuously updating the parameters to accurately represent all

Manuscript received October 4, 2012; revised January 7, 2013 and February 27, 2013; accepted March 22, 2013. Date of publication May 17, 2013; date of current version September 19, 2013. This work was supported in part by the National Science Foundation Award under Grant EEC-08212121.

H. Rahimi-Eichi and M.-Y. Chow are with North Carolina State University, Raleigh, NC 27606 USA (e-mail: hrahimi@ncsu.edu; chow@ncsu.edu).

F. Baronti is with the Dipartimento di Ingegneria dell'Informazione, University of Pisa, 56100 Pisa, Italy (e-mail: f.baronti@iet.unipi.it).

Color versions of one or more of the figures in this paper are available online at http://ieeexplore.ieee.org.

Digital Object Identifier 10.1109/TIE.2013.2263774

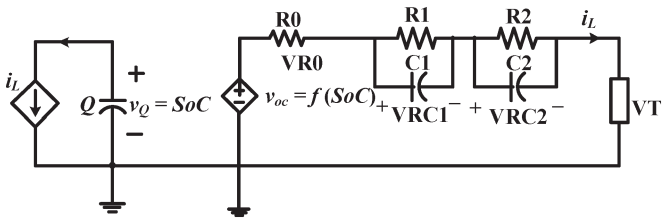

Fig. 1. Battery model with relaxation effect, internal resistance, and V_{OC}–SOC function.

of the battery's static and dynamic characteristics. Using this adaptive structure, we design an observer based on the updating model to estimate the SOC as one of the states of the battery model. In this paper, we use simulated and experimental data to assess the accuracy of the parameter-identification algorithm and its ability to track the changes in the parameters. At the same time, we are validating the premise of the battery's parameter changes with regard to different SOCs and different charging/discharging current rates. Moreover, we compare the results from the SOC coestimation to some of the famous existing algorithms (i.e., the Kalman filter and the sliding-mode observer). Although this algorithm is tailored for parameter identification and SOC estimation in a cell level, it can be easily expanded to be used in battery pack applications. That is because the battery pack consists of several battery cells in parallel or in series, and an aggregated model can be used to represent the pack behavior [15], [16].

In this paper, Section II describes the modeling of the battery; Section III explains the parameter-identification algorithm and the state observer design; Section IV verifies the efficacy of the identification algorithm to follow the changes in the battery parameters using simulated data; Section V talks about applying the online adaptive parameters/SOC coestimation approach to the experimental data; Section VI compares the different SOC estimation algorithms with one another; and Section VII concludes the paper.

II. Battery Model

Depending on the required accuracy and application, different types of models have been developed so far for the battery. Among those models, the RC-equivalent circuit is an effective model to represent the battery's dynamics. The following subsections describe some of the battery's characteristics that are considered in the model.

A. Linear Model With Internal Resistance

A typical rechargeable battery can, in first approximation, be modeled by a large capacitor that can store and release electrical energy during charging and discharging cycles. As in any electrochemical process, these charging/discharging cycles encounter a small resistance due to the electrolyte and the interphase resistance. This small resistance appears in series with the battery capacitor Q (internal resistor R_0 in Fig. 1). We note that the value of R_0 changes with the SOC, the ambient temperature, and the aging effect of the battery.

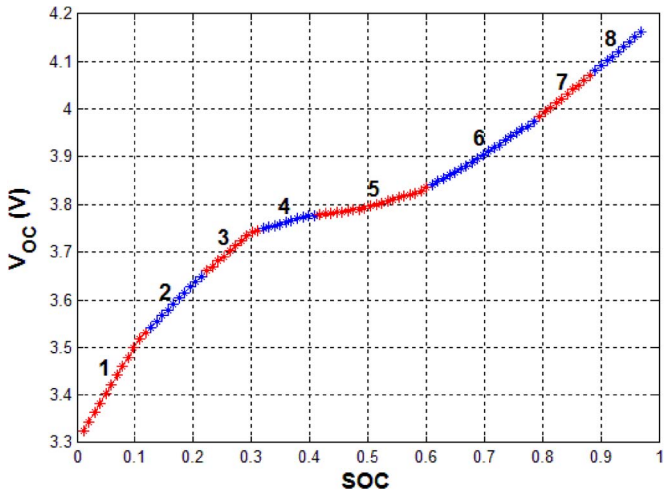

Fig. 2. Piecewise linear mapping of the V_{OC}–SOC curve.

B. Relaxation Effect

The relaxation effect is another basic characteristic of the battery that appears during and after the charging and discharging cycles. This effect represents the slow convergence of the battery's terminal voltage to its equilibrium after hours of relaxation following charging/discharging and is modeled by series-connected parallel RC circuits. The number of RC groups is a tradeoff between accuracy and complexity. While Chen and Rincon-Mora [17] recommended two RC groups as the optimal model, there are several references [11], [18], [19] stating that one RC group structure can provide results that are accurate enough for applications, such as PHEVs and PEVs. Temperature effect is another key factor that needs to be considered in the modeling of the battery. Its main manifestation is by the changes in the parameters of the battery model. As will be described in Section III, since the coestimation approach is based on the online identification of the parameters, the changes in the parameters caused by the temperature effect is embedded in the model, with the online identification of the parameters and the effect of temperature on the battery performance.

C. V_{OC}–SOC Relationship

Despite the simple linear model for the battery in Section II-A, the static relationship between V_{OC} and the SOC is intrinsically nonlinear. The nonlinearity of the model increases the complexity of the stability and performance analysis of the estimators. Therefore, considering the V_{OC}–SOC curve of the Li-polymer battery from experimental results, we show in [14] that it can be divided into eight linear segments, as demonstrated in Fig. 2, and each of them can be described by the following linear equation:

$$V_{OC} = f(\text{SOC}) = b_0 + b_1 \text{SOC}. \tag{1}$$

Fig. 3 describes how the linearized segments have been chosen by extracting the first and second derivatives of the V_{OC} versus the SOC. The spikes in Fig. 3(b) show the turning points that separate the piecewise linear regions. Afterward, using the least square (LS) error curve-fitting technique, the best lines to fit the segments are estimated. The values for b_0 and b_1

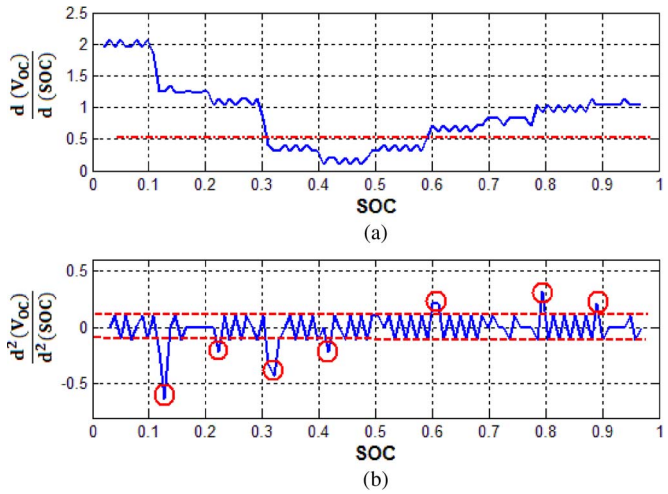

Fig. 3. (a) First and (b) second derivatives of V_{OC} versus the SOC.

TABLE I
PARAMETERS AND FITNESS OF PIECEWISE LINEAR SEGMENTS

Seg.\Param.	b_0	b_1	R^2
1	3.3046	1.9702	0.9991
2	3.3861	1.2348	0.9997
3	3.4299	1.0337	0.9945
4	3.6407	0.3389	0.9933
5	3.6479	0.3014	0.9667
6	3.3746	0.7604	0.9979
7	3.1981	0.9892	0.9998
8	3.1442	1.0509	0.9999

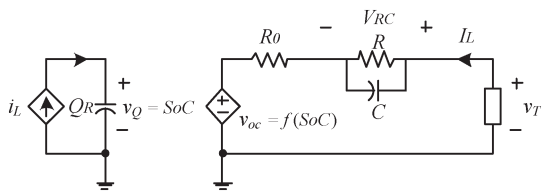

Fig. 4. Battery-equivalent circuit.

and the goodness-of-fit evaluation factor R^2 are derived and presented in Table I for each segment. The detailed rationale and justification of this approach have been described in [14].

D. State-Space Equations for the Model

To model the battery's characteristics, we used an RC-equivalent circuit, such as the one in Fig. 4, with one RC group to represent the relaxation effect. This simple model reduces the complexity of model identification and parameter extraction.

Considering the equivalent circuit for the battery model in Fig. 4 and (1), the state-space equations can be written as the following system to represent the battery's dynamics:

$$\begin{cases} \begin{bmatrix} \dot{\mathrm{SOC}} \\ \dot{V}_{RC} \end{bmatrix} = \begin{bmatrix} 0 & 0 \\ 0 & -\frac{1}{RC} \end{bmatrix} \begin{bmatrix} \mathrm{SOC} \\ V_{RC} \end{bmatrix} + \begin{bmatrix} 1/Q_R \\ 1/C \end{bmatrix} \mathrm{I_L} \\ V_T = \begin{bmatrix} b_1 & 1 \end{bmatrix} \begin{bmatrix} \mathrm{SOC} \\ V_{RC} \end{bmatrix} + R_0 I_L + b_0. \end{cases} \tag{2}$$

In these equations, the SOC of the battery and the voltage across the RC cell, i.e., V_{RC}, are selected to be the system-state variables. We assume that the terminal current (I_L) and voltage (V_T) are the only two values that are accessible from outside of system (2). To obtain the estimated SOC as one of the states, the parameters in the system need to be identified. We assume that Q_R is the nominal capacity of the battery. Hence, we need to estimate $\{b_0, R, C, R_0, b_1, S_{\mathrm{oc}}, V_{RC}\}$ as $\{\widehat{b}_0, \widehat{R}, \widehat{C}, \widehat{R}_0, \widehat{b}_1, \widehat{S}_{\mathrm{oc}}, \widehat{V}_{RC}\}$ using state estimation and system parameter-identification methods.

III. PARAMETER IDENTIFICATION AND SOC COESTIMATION

A. Moving Window LS

For online identification of the battery's parameters, we applied an adaptive parameter-identification algorithm to a linear system. The LS identification approach [20] provides a formula that minimizes the LS error between the estimated output value and the actual output at the present time step. Since the input/output samples are being updated step by step while the system is running, the recursive LS (RLS) [20] estimates the parameters of the system iteratively. Since implementing the RLS algorithm is not easy in an actual system and the input/output signal needs to be persistently exciting [20] at each step, we use the moving window LS method, which is more practical. In this approach, the input/output data corresponding to a certain number (window) of past steps is used to estimate the parameters. The length of the window depends on the excitation of the input signal to properly reveal the dynamics of the system.

B. Battery Parameter Identification

The parameters of the battery model that need to be estimated are: $\{b_0, R, C, R_0, b_1\}$. Since most of the parameter-identification methods for linear systems use the transfer function of the system to identify the parameters, we first obtain the following transfer function form of the system (2):

$$\frac{Y(s) - b_0}{U(s)} = \frac{R_0 s^2 + \left(\frac{b_1}{Q_R} + \frac{1}{C} + \frac{R_0}{RC}\right) s + \frac{b_1}{RCQ_R}}{s\left(s + \frac{1}{RC}\right)}. \tag{3}$$

From transfer function (3) and using a bilinear transform $(s \to (2/T)(z - 1/z + 1))$ [21], we can obtain the discrete transfer function of system (2) with sample time T, which leads us to the following transfer function, in which the coefficients are uniquely related to the battery parameters:

$$\frac{Y(z^{-1}) - b_0}{U(z^{-1})} = \frac{c_0 + c_1 z^{-1} + c_2 z^{-2}}{1 + a_1 z^{-1} + a_2 z^{-2}}. \tag{4}$$

The detailed equations to extract the battery parameters from the coefficients of transfer function (4) can be found in [14]. As shown in [14], despite the fact that the value of b_0 is not identifiable through this process, it acts like an output offset that does not influence the dynamics between the input and the output and enables other parameters to be uniquely identified.

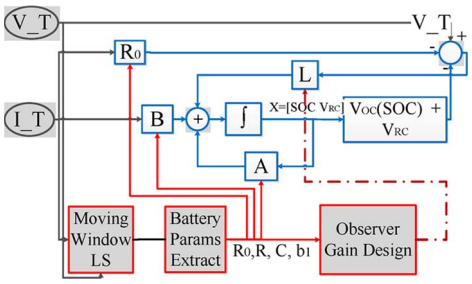

Fig. 5. Battery parameters/SOC coestimation block diagram.

C. Observer Design

After identifying the parameters of the battery, an observer is designed to estimate the SOC, which is one of the states of the model. Assuming that the battery's parameters $\{R, C, R_0, b_1, b_0\}$ can be estimated as $\{\widehat{R}, \widehat{C}, \widehat{R}_0, \widehat{b}_1, \widehat{b}_0\}$, the battery model is represented as a system with the following equations:

$$\begin{cases} \dot{x} = Ax + Bu \\ y = Cx + Du + b_0 \end{cases} \tag{5}$$

where $x_1 = S_{\rm oc}$, $x_2 = V_{RC}$,

$$A = \begin{bmatrix} 0 & 0 \\ 0 & -\frac{1}{RC} \end{bmatrix},$$

$$B = \begin{bmatrix} 1/Q_R \\ 1/C \end{bmatrix},$$

$C = [\,b_1 \quad 1\,]$, $D = R_0$, $u = I_L$, $y = V_T$, and

$$x = \begin{bmatrix} x_1 \\ x_2 \end{bmatrix}.$$

Therefore, the observer can be designed as a system with the following equations:

$$\begin{cases} \dot{\hat{x}} = A\hat{x} + Bu + L(y - \hat{y}) \\ \hat{y} = C\hat{x} + Du + b_0 \end{cases} \tag{6}$$

where $L^T = [L_1 \;\; L_2]$ is the observer gain vector. To design the observer gain, two methods can be used: the pole placement that we used in [14] and a linear quadratic (LQ) approach, in which an optimal observer is designed to minimize the error and effort. In this method, the P matrix is calculated by solving the following LQ Riccati equation:

$$AP + P^T A - PC^T R^{-1} CP = -Q \tag{7}$$

where Q and R are arbitrary semipositive- and positive-definite matrices, and the observer gain is obtained from the following equation:

$$L^T = R^{-1} CP. \tag{8}$$

Fig. 5 shows the block diagram that demonstrates the battery parameters/SOC coestimation algorithm. In this diagram, the moving window LS is used to identify the coefficients of the transfer function that represents the battery dynamics. The battery parameters are then extracted from the coefficients and fed to the observer to estimate the SOC of the battery. In this observer, the experimental look-up table is used to present the $V_{\rm OC}$–SOC relationship. Moreover, the LQ approach is employed to calculate the optimal observer gain based on the updated parameters.

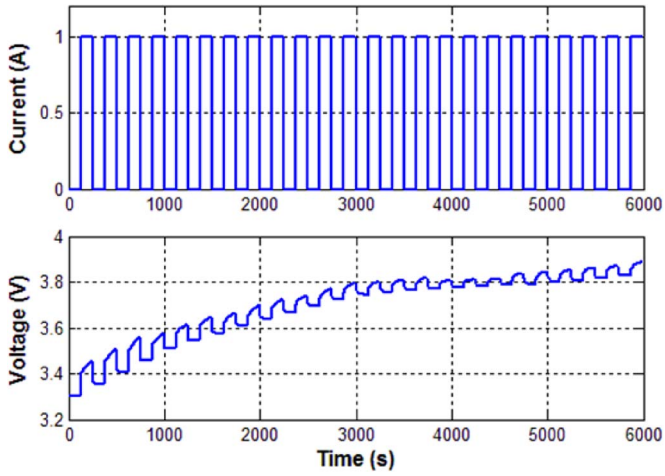

Fig. 6. Current and voltage of the battery model with changing parameters.

IV. Parameter-Identification Simulation Results

To verify the capability of the moving window LS identification algorithm to follow the changes in the battery parameters, we designed a simulation testbed. In this testbed, the input data (V_T and I_L) to the identification algorithm is provided by a battery model developed in SIMULINK, instead of actual measurements. The battery model is in the form of an RC-equivalent circuit similar to the one shown in Fig. 4, in which the $V_{\rm OC}$–SOC relationship is described with a look-up table that is obtained from the $V_{\rm OC}$–SOC experimental data measured on a lithium-polymer battery, as shown in Fig. 2. We applied the identification algorithm with a linear AutoRegressive with eXogenous input (ARX) structure to the intrinsically nonlinear model of the battery while the other battery parameters, such as R_0 and RC, change. With this test, we make sure that the identified changes in the battery parameters are caused by actual changes in the battery parameters and not by the nonlinearity of the system.

To do so, we apply 1-A current pulses with a pulsewidth of 125 s followed by the same amount of resting time to the battery model with a look-up table to represent the actual $V_{\rm OC}$–SOC relationship. At the same time, the battery's parameters, which are basically R_0, R, and C, change over time according to the actual behavior of the battery, as it comes from experiments carried out in similar conditions. Fig. 6 shows the simulated terminal voltage of the battery with the corresponding terminal current. Applying the moving LS parameter-identification algorithm to the current and voltage signals as the system's input and output, the parameters of the battery are estimated online at each simulation time. The main battery parameters (i.e., R_0, RC, and R) are shown in Fig. 7 compared with their actual values. The identification results show that the algorithm is able to follow the changes in the parameters accurately after a short

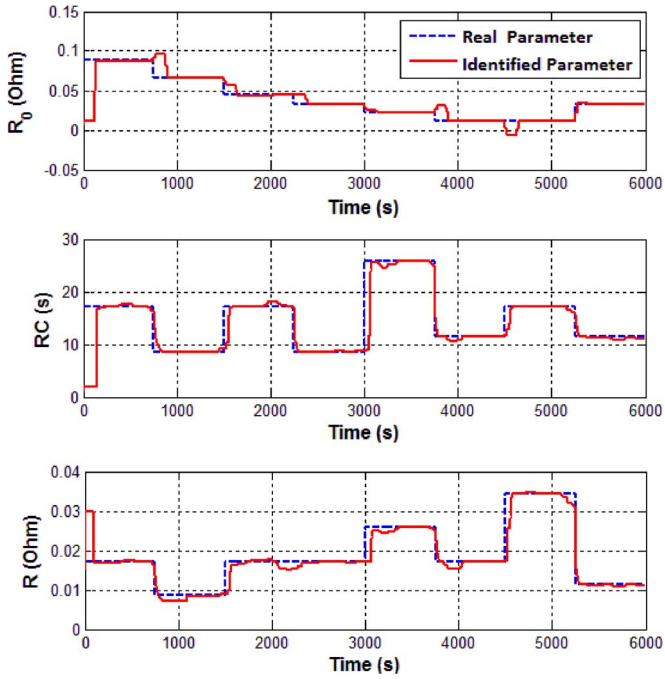

Fig. 7. Parameter-identification results for the nonlinear battery model.

transition time. This amount of time is mostly related to the width of the current signal pulses because the algorithm needs to detect a step-down or a step-up in the input signal window to identify the new parameters. Moreover, some deviations from the actual values after convergence are caused by switching from one V_{OC}–SOC linear region to another, and the identification error is removed afterward. However, Fig. 7 shows that we can trust the results of the parameter-identification algorithm despite the inherent nonlinearity of the battery model, and we can use the online-estimated parameters to examine our models for changes in the parameters with regard to the SOC, C-rate, and temperature effect.

V. Experimental Results

After testing the parameter-identification algorithm with simulated data, in the next step, we applied the algorithm to the experimental battery data, aiming to show the performance under real application conditions. The experimental data were acquired on 1.5-Ah Li-polymer cells (Kokam SLPB723870H4). These cells feature a specific energy density of 150 Wh/kg and can continuously be charged and discharged within the 2.7- and 4.2-V voltage range with currents up to 3 A for charge and 30 A for discharge. The experimental setup, as shown in Fig. 8, was the analog of the one described in [14] and [22] and allowed us to validate the proposed coestimation algorithm in many battery conditions, controlling the charge/discharging rate, as well as the cell temperature. In Fig. 8, starting from the left-hand side of the image, we can see the temperature-controlled chamber used to regulate the battery temperature; a power supply and an electronic load, which set the charging/discharging current of the battery. All the equipment, as well as the acquisition process, are controlled by a LabVIEW application, whose panel is shown on the screen in the picture.

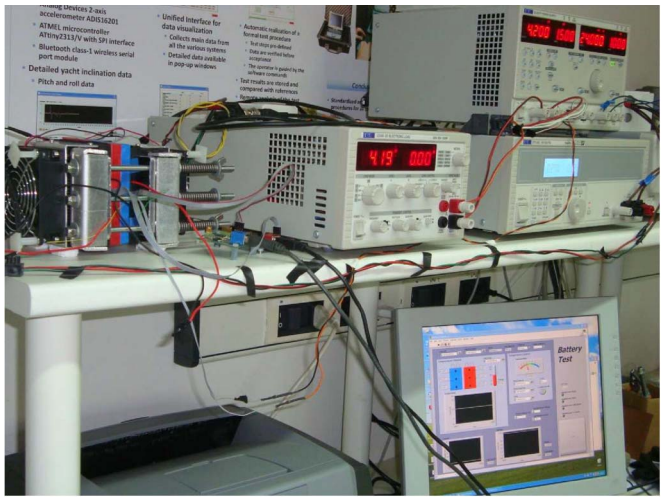

Fig. 8. Experimental setup.

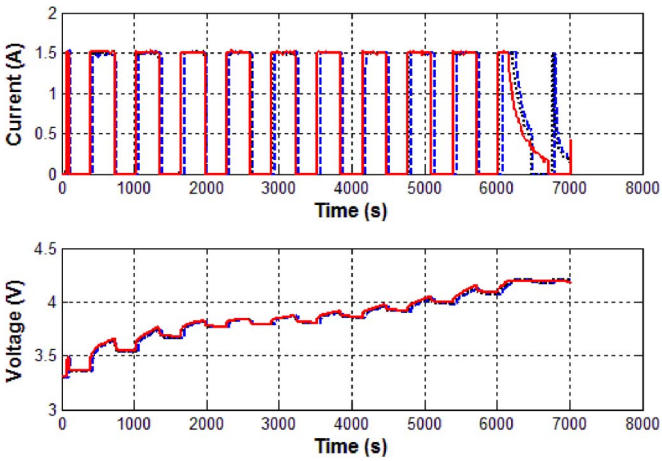

Fig. 9. Current and voltage signals for three pulse-charging tests with the same current rates.

As a significant example, in Fig. 9, we report the current and voltage data of three runs of the same pulse-charging test performed at 1 C-rate (i.e., a charging current equal to the capacity value in amperes) and 25 °C. Since these similar data contain different noise and battery chemical conditions, analysis of the identified battery parameters helped us to verify the robustness of the battery parameter-identification method and to further validate our conclusions about the changing dynamics of the battery model. Therefore, applying the same identification algorithm to the input and output data, the parameters of the battery, i.e., R_0, RC, and b_1, are identified. Fig. 10 shows the behavior of the estimated parameters versus SOC. We can see from the first graph in Fig. 10 that R_0 is, as expected, larger at lower SOCs and it decreases down to 1/8 of the initial value when the battery is fully charged. The changes in RC, and consequently R and C, are more irregular than R_0 due to the fact that RC is more dependent on the chemical reactions of the battery during charge and discharge. Another explanation for this irregularity is that the relaxation effect requires several RC groups to be accurately modeled. For a practical application, when we use just one RC group, the estimated value converges to different time constants to provide

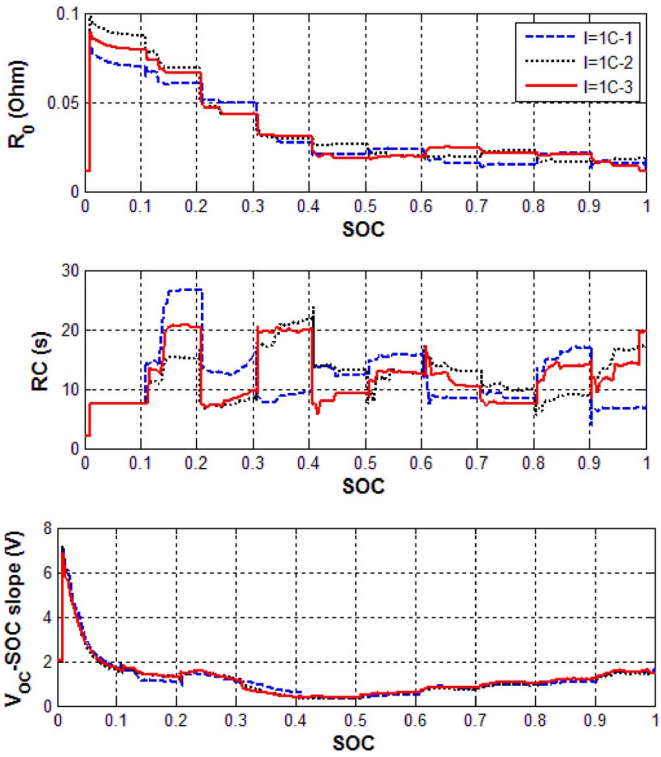

Fig. 10. Identified parameters obtained from three independent tests with the same charging rates.

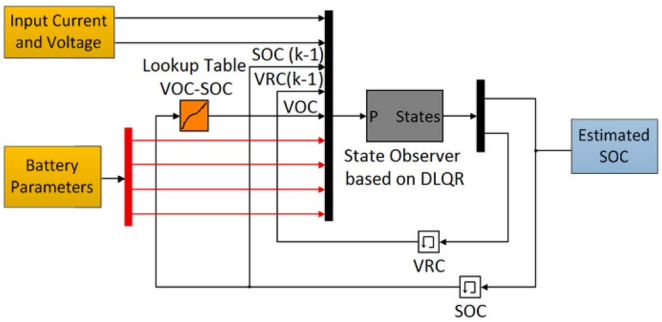

Fig. 11. MATLAB/SIMULINK implementation of the SOC coestimation observer.

a better approximation of the actual electrochemical condition. The third graph in Fig. 10 reports the estimated $V_{\rm OC}$–SOC slope (b_1). Although the slope changes with the SOC, the identified value is almost the same for the three tests. This proves the very good repeatability of the static battery behavior represented by the $V_{\rm OC}$–SOC curve.

After identifying the battery parameters, we apply the discrete version of the LQ observer to design the observer to estimate the SOC of the battery. As we previously demonstrated in Fig. 2, the $V_{\rm OC}$–SOC relationship function is nonlinear in the structure of the observer, and we used a look-up table that is obtained from experimental data to represent this function. Fig. 11 shows how the algorithm is implemented in SIMULINK. The SOC and V_{RC} values estimated at the previous time step are fed back to the algorithm core to estimate the new values. In addition, the SOC is used to find $V_{\rm OC}$ through the look-up table. Moreover, identified parameters are injected into the algorithm

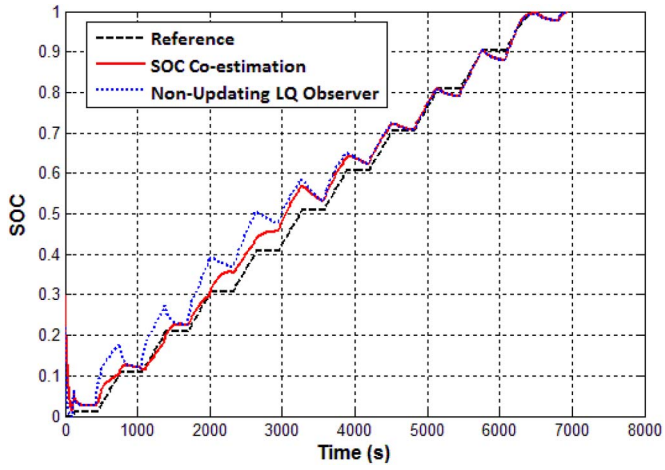

Fig. 12. SOC estimation results with updating (SOC coestimation) and nonupdating observers.

to update the model continuously. In practical applications, the updating frequency of the parameters depends on the characteristics of the application, including the charging/discharging rate and environmental conditions.

Therefore, while we update the parameters at each sample time to observe the details, the updating can be done much less frequently to minimize the computational time and memory needed. The SOC estimation results, as shown in Fig. 12, demonstrate the performance of the coestimation algorithm compared to the nonupdating LQ observer. Both of the SOC estimation results are compared with the benchmark value for the real SOC, which is obtained from coulomb counting with a known initial SOC and ignoring any sensor errors. The results show that the nonupdating observer generates more errors, particularly in the region with the lower SOC, than the updating observer. To evaluate the performance of the algorithms, we use two norms of the error, namely, $\|e\|_2$ and $\|e\|_\infty$, which are defined as follows:

$$\|e\|_2 = \sqrt{\frac{1}{K}\sum_{k=1}^{K} e^2(k)} \tag{9}$$

$$\|e\|_\infty = \max_k |e(k)|\,. \tag{10}$$

Moreover, we define the convergence time of the estimation as the first time that the estimated SOC enters the 5% error bound compared with the reference SOC.

Fig. 13 demonstrates $\|e\|_2$ for both approaches and shows that the rate of increase in the norm for the nonupdating observer is large for small SOCs, whereas for the updating observer (coestimation approach), the increasing rate is small for most of the SOC range. The only region where we see more errors in the estimation of the coestimation method is between 2000 and 4000 s, which corresponds to an SOC between 0.3 and 0.6. This region, as shown in Fig. 3(a), is the one with a $V_{\rm OC}$–SOC slope of less than 0.5. In [23], we have shown that a small $V_{\rm OC}$–SOC slope has a significant influence on the observability of the battery model's states. Finally, in order to better demonstrate the influence of identifying and updating the

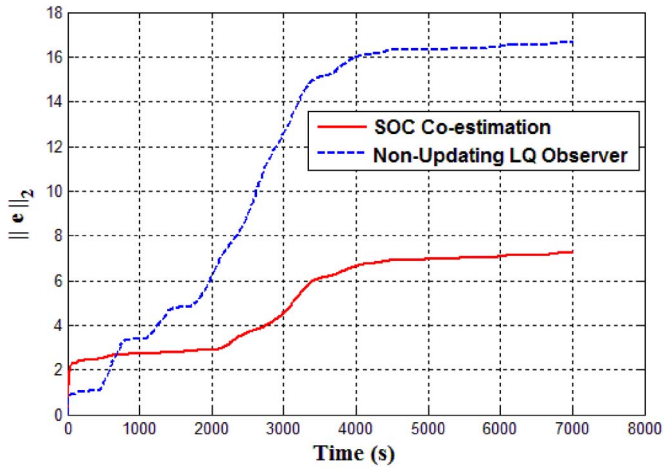

Fig. 13. $\|e\|_2$ for updating and nonupdating observers.

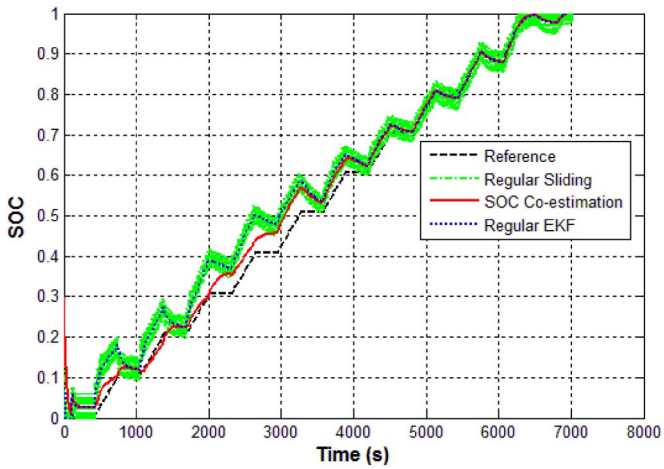

Fig. 14. Comparison of the SOC estimation results for different algorithms.

TABLE II
COMPARISON OF SOC ESTIMATION RESULTS FOR UPDATING AND NONUPDATING OBSERVERS

	SOC Co-Estimation	Non-Updating LQ Observer
$\|e\|_2$	7.239	16.64
$\|e\|_\infty$	0.06395	0.09985
Convergence Time (s)	60	30

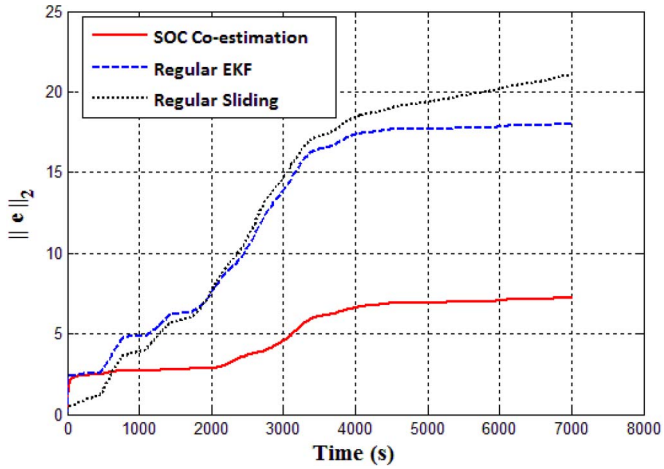

Fig. 15. Comparison of the $\|e\|_2$ of the errors for different algorithms.

battery parameters in the SOC estimation, Table II presents the $\|e\|_2$, $\|e\|_\infty$, and convergence time for both cases. As expected, both error indicators are significantly smaller when the parameters are updated in the coestimation method. In contrast, the convergence time is larger for the coestimation approach due to the slow convergence of the parameter-identification algorithm.

VI. COMPARISON OF SOC ESTIMATION ALGORITHMS

To evaluate the performance and accuracy of the online battery parameters/SOC estimation algorithm, we compare the results to the ones obtained from two of the recently popular algorithms, namely, the extended Kalman filter (EKF) and the sliding-mode observer. While both of those algorithms are based on designing an observer for the battery model, the Kalman filter considers the uncertainty of the model as state noise and designs an adaptive filter to minimize the noise effect. The EKF is the nonlinear version of the Kalman filter, in which the nonlinear system is linearized at the operating point, and an optimal gain is designed based on the linearized model to minimize the noise effect on the state. Similarly, for the sliding-mode observer, a linearized system at the operating point is considered to be the main model for the battery, and the nonlinearities in the actual battery are presented as additive uncertainties to the model. Consequently, to design an observer gain for optimal performance of the linearized model, a sliding-mode gain is added to compensate for the uncertainties. The key point for both the EKF and the sliding-mode observer is that the observer design is based on a fixed model of the battery, in which the coefficients are obtained from offline identification of the battery's parameters. Therefore, according to the changes in the battery's parameters at different SOCs and charging/discharging rates, we expect that the SOC estimation with these algorithms cannot provide accurate results compared with the parameters/SOC coestimation algorithm.

To compare the performance of these algorithms, we implemented both of them in SIMULINK. Again, for the nonlinear relationship between $V_{\rm OC}$ and the SOC, we used a look-up table in the structure of the observers to increase the accuracy. The SOC estimation results are demonstrated in Fig. 14, in which the results for the sliding-mode observer, EKF, and SOC coestimation are compared with each other. We can see that the SOC estimation for the EKF is very close to the one in Fig. 12 for a nonupdating LQ observer. The SOC estimation shows more error from the real SOC when the battery parameters (particularly R_0) are different from the offline identified parameters. For the sliding-mode observer, the SOC estimation fluctuates around the estimated values that are close to the EKF. Although the fluctuation causes the results to approach the real SOC at some points, most of the time it produces a larger steady-state error. Fig. 15, which shows the $\|e\|_2$ of the error for three algorithms, confirms that, although the sliding mode gives better results than the EKF for small SOCs (i.e., up to 0.3), the permanent error caused by the fluctuation retreats for the larger SOCs. However, the significant difference between the error for the parameters/SOC coestimation algorithm and the other two algorithms that are based on offline identification

TABLE III
QUANTITATIVE COMPARISON OF DIFFERENT ALGORITHMS

	SOC Co-estimation	Regular EKF	Regular Sliding
$\|e\|_2$	7.239	18.01	21.07
$\|e\|_\infty$	0.06395	0.07771	0.1219
Convergence Time (s)	60	20	15

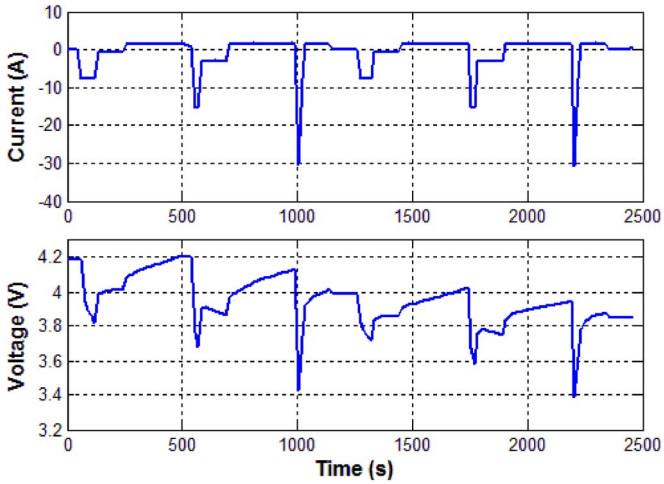

Fig. 16. Generic current and voltage profiles.

of battery parameters implies that online identification and updating the battery parameters are crucial to obtain accurate SOC estimation results. The values for $\|e\|_2$, $\|e\|_\infty$, and convergence time, which are demonstrated in Table III, describe the quantitative differences between the performances of the three algorithms. Table III shows that, in $\|e\|_2$, which evaluates the history of the error, the gap between the coestimation and the other two algorithms with nonupdating parameters is meaningful. However, for $\|e\|_\infty$, which presents the maximum error, the EKF is close to the coestimation and the sliding mode suffers from a significantly large maximum estimation error because of the fluctuations. According to these results, we can expect that updating the battery parameters in the structure of the EKF and the sliding-mode observer remarkably improves the performance of those algorithms. Again, we can see that the convergence time is larger for the SOC coestimation algorithm due to the time needed to update the parameters.

Moreover, to compare the performance of the three algorithms, with regard to a realistic scenario, we used a typical current profile such as the one represented in Fig. 16 along with the corresponding voltage profile. This current profile contains both charging and discharging cycles, as well as different discharging rates up to 30 A (20 C), for the same lithium-polymer battery cell. After applying the three SOC estimation algorithms to the current and voltage data, the estimation results are demonstrated in Fig. 17. We can see that, although the estimation error is larger in this case, due to the changes in current value and direction, the SOC coestimation shows a better performance in estimating the reference SOC value. Table IV shows the quantitative comparison of the three algorithms' performance in terms of $\|e\|_2$, $\|e\|_\infty$, and convergence time for the typical profile scenario. Again, the small values

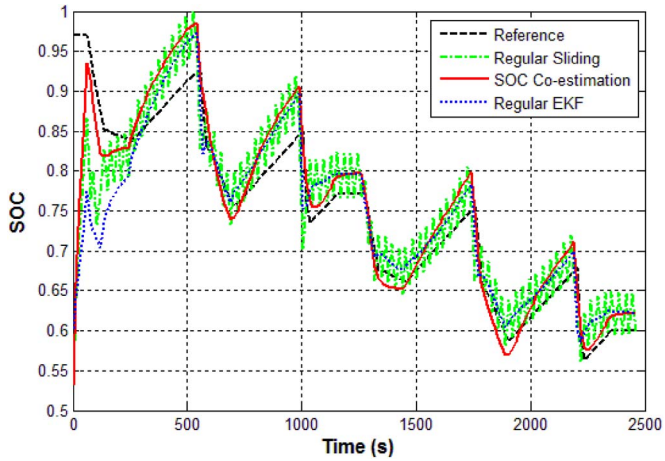

Fig. 17. Comparison of the SOC estimation results for the generic current profile scenario.

TABLE IV
QUANTITATIVE COMPARISON OF ALGORITHMS FOR GENERIC PROFILE SCENARIO

	SOC Co-estimation	Regular EKF	Regular Sliding
$\|e\|_2$	7.45	11.24	11.59
$\|e\|_\infty$	0.0645	0.0988	0.1488
Convergence Time (s)	60	240	135

for the $\|e\|_2$ and $\|e\|_\infty$ for the SOC coestimation compared with the other algorithms confirms the need for updating the battery parameters in the observer structure. Moreover, the SOC coestimation algorithm shows a better performance in terms of convergence time in this case. That is because the observers in the nonupdating algorithms, i.e., EKF and sliding mode, need more time to converge to the correct SOC due to the changes in the current profile, whereas the SOC coestimation adapts to the changes more quickly.

VII. CONCLUSION

In order to estimate the SOC of the battery, the RC-equivalent circuit is used to model the dynamics of the battery. Since the parameters of the battery model are functions of the SOC, C-rate, temperature, and aging, all of the parameters are subject to change and need to be identified with a proper frequency during the SOC estimation. Most of the observer-based SOC estimation algorithms proposed so far design the state observer based on a model with fixed parameters that are obtained from offline identification. In this paper, we have shown that changing the parameters of the battery needs to be identified and the observer structure updated to provide an accurate SOC estimation. To do that online, the adaptive battery parameters/SOC coestimation approach was proposed, in which a piecewise linear mapping of the $V_{\rm OC}$–SOC function was used to identify the battery parameters and feed them to an optimal observer to estimate the SOC. We verified the performance of the parameter-identification algorithm by applying it to simulated and experimental data. The necessity of updating the parameters in the observer structure was verified with the

results of the experimental data. Moreover, the performance of the SOC coestimation algorithm was compared with the EKF and the sliding-mode observer as two popular SOC estimation approaches. All of the results indicate that updating the parameters of the battery model during SOC estimation is key to increase the accuracy of the estimation and avoid unnecessary compensation for uncertainties.

REFERENCES

[1] K. S. Ng, C.-S. Moo, Y.-P. Chen, and Y.-C. Hsieh, "Enhanced coulomb counting method for estimating state-of-charge and state-of-health of lithium-ion batteries," *Appl. Energy*, vol. 86, no. 9, pp. 1506–1511, Sep. 2009.

[2] M. Coleman, L. Chi Kwan, Z. Chunbo, and W. G. Hurley, "State-of-charge determination from EMF voltage estimation: Using impedance, terminal voltage, and current for lead-acid and lithium-ion batteries," *IEEE Trans. Ind. Electron.*, vol. 54, no. 5, pp. 2550–2557, Oct. 2007.

[3] F. Codeca, S. M. Savaresi, and V. Manzoni, "The mix estimation algorithm for battery state-of-charge estimator—Analysis of the sensitivity to measurement errors," in *Proc. 48th IEEE CDC/CCC*, Shanghai, China, Dec. 15–18, 2009, pp. 8083–8088.

[4] R. Li, J. Wu, H. Wang, and G. Li, "Prediction of state of charge of lithium-ion rechargeable battery with electrochemical impedance spectroscopy theory," in *Proc. 5th IEEE ICIEA*, Taichung, Taiwan, Jun. 15–17, 2010, pp. 684–688.

[5] A. Zenati, P. Desprez, and H. Razik, "Estimation of the SOC and the SOH of Li-ion batteries, by combining impedance measurements with the fuzzy logic inference," in *Proc. 36th Annu. Conf. IEEE IECON*, Glendale, AZ, USA, Nov. 7–10, 2010, pp. 1773–1778.

[6] G. L. Plett, "Extended Kalman filtering for battery management systems of LiPB-based HEV battery packs—Part 2. Modeling and identification," *J. Power Sources*, vol. 134, no. 2, pp. 262–276, Aug. 2004.

[7] M. Shahriari and M. Farrokhi, "Online state-of-health estimation of VRLA batteries using state of charge," *IEEE Trans. Ind. Electron.*, vol. 60, no. 1, pp. 191–202, Jan. 2013.

[8] M. Charkhgard and M. Farrokhi, "State-of-charge estimation for lithium-ion batteries using neural networks and EKF," *IEEE Trans. Ind. Electron.*, vol. 57, no. 12, pp. 4178–4187, Dec. 2010.

[9] B. S. Bhangu, P. Bentley, D. A. Stone, and C. M. Bingham, "Nonlinear observers for predicting state-of-charge and state-of-health of lead-acid batteries for hybrid-electric vehicles," *IEEE Trans. Veh. Technol.*, vol. 54, no. 3, pp. 783–794, May 2005.

[10] I.-S. Kim, "Nonlinear state of charge estimator for hybrid electric vehicle battery," *IEEE Trans. Power Electron.*, vol. 23, no. 4, pp. 2027–2034, Jul. 2008.

[11] I.-S. Kim, "A technique for estimating the state of health of lithium batteries through a dual-sliding-mode observer," *IEEE Trans. Power Electron.*, vol. 25, no. 4, pp. 1013–1022, Apr. 2010.

[12] F. Zhang, G. Liu, and L. Fang, "A battery state of charge estimation method using sliding mode observer," in *Proc. 7th WCICA*, Chongqing, China, Jun. 25–27, 2008, pp. 989–994.

[13] F. Zhang, G. Liu, L. Fang, and H. Wang, "Estimation of battery state of charge with H observer: Applied to a robot for inspecting power transmission lines," *IEEE Trans. Ind. Electron.*, vol. 59, no. 2, pp. 1086–1095, Feb. 2012.

[14] H. Rahimi-Eichi, F. Baronti, and M. Y. Chow, "Modeling and online parameter identification of Li-Polymer battery cells for SOC estimation," in *Proc. IEEE ISIE*, 2012, pp. 1336–1341.

[15] H. Li, C. Liao, and L. Wang, "Research on state-of-charge estimation of battery pack used on hybrid electric vehicle," in *Proc. APPEEC*, Wuhan, China, Mar. 27–31, 2009, pp. 1–4.

[16] Y. Liaoa, J. Huanga, and Q. Zenga, "A novel method for estimating state of charge of lithium ion battery packs," in *Proc. ICAMMP*, Shenzhen, China, 2011, pp. 428–435.

[17] M. Chen and G. A. Rincon-Mora, "Accurate electrical battery model capable of predicting runtime and I–V performance," *IEEE Trans. Energy Convers.*, vol. 21, no. 2, pp. 504–511, Jun. 2006.

[18] C. R. Gould, C. M. Bingham, D. A. Stone, and P. Bentley, "New battery model and state-of-health determination through subspace parameter estimation and state-observer techniques," *IEEE Trans. Veh. Technol.*, vol. 58, no. 8, pp. 3905–3916, Oct. 2009.

[19] M. A. Roscher and D. U. Sauer, "Dynamic electric behavior and open-circuit-voltage modeling of LiFePO4-based lithium ion secondary batteries," *J. Power Sources*, vol. 196, no. 1, pp. 331–336, Jan. 2011.

[20] K. J. Astrom and B. Wittenmark, *Adaptive Control*, 2nd ed. Englewood Cliffs, NJ, USA: Prentice-Hall, 1994.

[21] K. Ogata, *Discrete-Time Control Systems*. Englewood Cliffs, NJ, USA: Prentice-Hall, 1986.

[22] F. Baronti, G. Fantechi, E. Leonardi, R. Roncella, and R. Saletti, "Enhanced model for lithium-polymer cells including temperature effects," in *Proc. 36th Annu. Conf. IEEE IECON*, 2010, pp. 2329–2333.

[23] H. Rahimi-Eichi and M.-Y. Chow, "Adaptive parameter identification and state-of-charge estimation of lithium-ion batteries," in *Proc. 38th Annu. Conf. IEEE Ind. Electron. Soc.*, Montreal, QC, Canada, 2012, pp. 4012–4017.

Habiballah Rahimi-Eichi (S'08) received the B.Sc. degree in electrical engineering from the Isfahan University of Technology, Isfahan, Iran, and the M.Sc. degree in electrical engineering from the Khaje Nasir Toosi University of Technology, Tehran, Iran, where he specialized in adaptive and robust control. He is currently working toward the Ph.D. degree at North Carolina State University, Raleigh, NC, USA, focusing on online state-of-charge and state-of-health monitoring of batteries, particularly in electric vehicles and smart grid applications.

He is currently a Research Assistant with the Advanced Diagnosis Automation and Control Laboratory, North Carolina State University. He has publications on adaptive modeling, parameter identification, and state estimation of different battery types.

Mr. Rahimi-Eichi is a member of the IEEE Industrial Electronics Society.

Federico Baronti (M'08) received the M.Sc. and Ph.D. degrees in electronic engineering from the University of Pisa, Pisa, Italy, in 2001 and 2005, respectively.

He is currently an Assistant Professor with the Dipartimento di Ingegneria dell'Informazione, University of Pisa, Pisa. His research interests include the design of embedded electronic systems for biomedical, automotive, and marine applications, as well as multichannel data acquisition and processing systems. His recent research has been focused on Li-ion battery modeling and the development of novel battery monitoring and management systems. In this area, he has collaborated on national and European projects.

Dr. Baronti is a member of the IEEE Industrial Electronics Society.

Mo-Yuen Chow (S'81–M'82–SM'93–F'07) received the Ph.D. degree from Cornell University, Ithaca, NY, USA, in 1987.

He is currently a Professor with North Carolina State University, Raleigh, NC, USA, where he is the Founder and Director of the Advanced Diagnosis Automation and Control Laboratory. He is also a Changjiang Scholar Professor with Zhejiang University, Hangzhou, China. He has published one book, several book chapters, and over 200 journal and conference articles related to his research work. His current research focuses on cooperative distributed control and fault management with applications on smart grids, plug-in hybrid electric vehicles, batteries, and mechatronics systems.

Dr. Chow was the Editor-in-Chief of the IEEE TRANSACTIONS ON INDUSTRIAL ELECTRONICS from 2010 to 2012. He was the recipient of the IEEE Region-3 Joseph M. Biedenbach Outstanding Engineering Educator Award.